ELSEVIER

Intermetallics 7 (1999) 611–620

Intermetallics

Synthesis and properties of Mo_5Si_3 single crystals

F. Chu *, D.J. Thoma, K. McClellan, P. Peralta, Y. He †

Materials Science and Technology Division, Mail Stop G755, Los Alamos National Laboratory, Los Alamos, NM 87545, USA

Received 2 February 1998; accepted 17 March 1998

Abstract

The ultra-high temperature structural intermetallic Mo_5Si_3 has been studied for alloy processing, physical properties, and mechanical behavior. High purity single crystals of Mo_5Si_3 have been synthesized by both optical floating zone and Czochralski methods. Structural, thermal, and elastic properties of Mo_5Si_3 single crystals were measured by X-ray powder diffraction, thermal mechanical analysis, and resonant ultrasound spectroscopy, respectively. Results show that the thermal expansion of Mo_5Si_3, a tetragonal structure with I4/*mcm* symmetry, is strongly anisotropic along the **a** and **c** directions with $\alpha_c/\alpha_a = 2.2$. Single crystal elastic moduli of Mo_5Si_3 indicate that it has less elastic anisotropy and lower shear modulus than most transition metal disilicides. The impacts of these physical properties on alloy processing and mechanical behavior are discussed. Room temperature Vickers indentation tests on the (100) and (001) planes have been performed for different orientations of the indenter diagonal and the corresponding hardness, fracture toughness, and deformation behavior have been obtained as a function of the crystallography. Finally, the physical properties and mechanical behavior of Mo_5Si_3 are compared with those of other high temperature structural silicides, e.g. $MoSi_2$.

Keywords: A. Molybdenum silicides; B. Mechanical properties at ambient temperatures; B. Thermal properties; C. Crystal growth

1. Introduction

High temperature structural applications require materials with a high melting point, high strength, good oxidation resistance, and excellent creep behavior at elevated temperatures. Many intermetalllic phases offer these desired properties, e.g. nickel aluminides, [1–3] titanium aluminides, [4] transition metal disilicides, [3,5,6] and Laves phase alloys. [7] Among these phases, refractory metal silicides appear to be more attractive because of their ultra-high melting temperatures and excellent oxidation resistance. [4]

For the refractory metal silicides, the intermetallic phases in the Mo–Si system show promising potentials because Mo has a lower density compared to other refractory metals and Mo does not embrittle with oxygen and nitrogen volatilization. In the Mo–Si system, there are three intermetallic phases, i.e. $C11_b$-structured $MoSi_2$, D_{8m}-structured Mo_5Si_3, and A15-structured Mo_3Si. [8] $MoSi_2$ has been studied extensively as a potential high temperature structural material. Mo_5Si_3 and Mo_3Si are receiving more attention recently in studies of their physical properties and mechanical behavior.

Mo_5Si_3 belongs to the space group I4/*mcm* (140). As a body-centered tetragonal lattice (tI32), it has 20 Mo atoms and 12 Si atoms in the unit cell. Mo_5Si_3 has the following structural characteristics: (1) its **a**-lattice parameter is larger than its **c**-lattice parameter ($a/c \sim 2$), which is different from those of typical tetragonal high temperature structural intermetallics, e.g. $MoSi_2$ and TiAl; (2) it has no close-packed planes, which is also different from those of the typical tetragonal high temperature structural intermetallics, e.g. $MoSi_2$ and TiAl; and (3) the –Si–Mo–Si– chains in Mo_5Si_3 are along [100] and [010] directions (these chains may also be along other directions, e.g. < 331]) and the –Mo–Mo– and –Si–Si– chains are along [001] direction. On the other hand, the –Si–Mo–Si– chains in $MoSi_2$ are along [001] direction and the –Mo–Mo– and –Si–Si– chains are along [100] and [010] directions. It is believed, in general, that the interatomic bonding strength of the –Si–Mo–Si– chains is stronger than those of the –Mo–Mo– and –Si–Si– chains. Mo_5Si_3 has a very high melting point of 2180°C, [8] which is substantially higher than that of $MoSi_2$ (2020°C) and a reasonable density of 8.19 g cm^{-3},

* Corresponding author

† Present address: Intel Corporation, Assembly/Test Materials Operation, MS CH5-232, Chandler, AZ 85226, USA

0966-9795/99/$—see front matter
PII: S0966-9795(98)00059-4

which is higher than that of $MoSi_2$ (6.3 g cm^{-3}). Therefore, it is considered as a promising ultra-high temperature structural material. In addition, Mo_5Si_3 has a relatively large range of nonstoichiometry (2–3 at.%), compared to $MoSi_2$ which is basically a line compound, according to the Mo–Si phase diagram. [8]

Owing to the potential advantages of Mo_5Si_3, either in monolithic or multi-phase systems, detailed studies for the fundamental physical–mechanical properties have been initiated. This first report explores the synthesis of high-quality single crystals and the measurement of physical and mechanical properties. In Section 2, the experimental procedures are outlined. Main results and discussion are presented in Section 3, including the fabrication of Mo_5Si_3 single crystals and their structural, thermal, elastic and mechanical properties. Finally, conclusions are drawn in Section 4.

2. Experimental procedures

2.1. Synthesis of the Mo_5Si_3 single crystals

Elemental Mo and Si with nominal purities of 99.97 at.% and 99.95 at.% were chemically cleaned before alloying. Mo_5Si_3 alloys were made in the form of arc-melted buttons and rods by arc-melting. In the process, the alloys were turned over and melted three times in an argon atmosphere in order to ensure chemical homogeneity.

Single crystals of Mo_5Si_3 were grown by the optical floating zone technique using arc-melted rods and by the Czochralski method using a tri-arc crystal growth furnace and arc-melted buttons. In the optical floating zone method, a dual-mirror system with 3.5 kW lamps was used. Typical rotation rates for both the seed crystal and feed rod were 30–40 rpm. The crystals were grown at a rate of 7 mm h^{-1}. In the Czochralski method, typical rotation rates for both the crystal and melt were about 20 rpm and the crystals were grown at a rate of 11 mm h^{-1}. In order to prevent oxidation and silicon evaporation, the single crystal growth was carried out under ~10 psi pressure of flowing ultra-high purity argon atmosphere for both methods.

Chemical analysis was conducted for both the as-melted polycrystals and the as-grown single crystals of Mo_5Si_3. In this analysis, the Mo and Si contents were analyzed by direct current plasma emission spectroscopy. The oxygen and nitrogen contents were characterized by inert gas fusion experiments.

2.2. Measurement of the physical properties of Mo_5Si_3

Using these crystals, the structural, thermal and elastic properties of Mo_5Si_3 were measured. In the structural property study, X-ray powder diffraction (XRD) experiments were performed on powder samples made from as-melted alloys to precisely determine its crystal structure and lattice parameters. The XRD patterns were obtained with a Scintag X-ray diffractometer (Cu $K_{\alpha 1}$ radiation with $\lambda = 0.15406$ nm) at room temperature. The lattice parameters were determined from a least-square fit.

In the thermal property investigation, the thermal expansion of single crystal Mo_5Si_3 was examined using a Perkin-Elmer DMA-7 thermal mechanical analyzer (TMA) operated in TMA mode in the regime 298–773K. The coefficients of thermal expansion (CTE) along the **a** and **c** axes were measured on a rectangular parallelepiped specimen (5 mm [100]×5 mm [010]×4 mm [001]), which was cut using a diamond wafer blade from the as-grown single crystal after orienting it using the Laue back reflection technique and polished using SiC papers and lapping films. The CTE along the **a** axis was obtained from the measurement along the larger dimension (5 mm) and the CTE along the **c** axis was obtained from the measurement along the shorter dimension (4 mm).

The room temperature single crystal elastic moduli of Mo_5Si_3 were measured by resonant ultrasound spectroscopy (RUS). [9] The single crystal Mo_5Si_3 specimen was cut and polished, as described above, into a rectangular parallelepiped geometry with dimensions $x_1 = 3.217 \pm 0.002$ mm, $x_2 = 2.950 \pm 0.001$ mm, and $x_3 = 3.702 \pm 0.003$ mm. The Laue back reflection X-ray technique was used to orient $\mathbf{x}_1$ parallel to [100], $\mathbf{x}_2$ parallel to [010] and $\mathbf{x}_3$ parallel to [001]. The mass density of the specimen was determined from its dimensions and mass. The room temperature single crystal elastic moduli were determined using 70 resonant frequencies from 0.45–1.82 MHz. Using these elastic constants, the elastic Debye temperature (Θ_D) of Mo_5Si_3 can be calculated from the relationship: [10]

$$\Theta_D = \frac{h}{k_B}\left(\frac{3N_0}{4\pi V}\right)^{1/3} v_m \tag{1}$$

Here, h and k_B denote the Planck and Boltzmann constants; N_0 is the number of independent three-dimensional oscillators in a volume V; and v_m denotes the mean sound velocity defined by:

$$v_m^{-3} = \frac{1}{M}\sum_{i=1}^{M}\frac{1}{3}\left(v_{li}^{-3} + 2v_{ti}^{-3}\right) \tag{2}$$

where v_{li} and v_{ti} indicate longitudinal and transverse velocities in the ith propagating direction, respectively, and M is the number of all propagating directions. For this study, we chose $M = 70$. v_l and v_t can be determined

from the measured c_{ij} and mass-density by solving the usual Christoffel equations [10] in the relevant propagation direction.

2.3. Characterization of the mechanical properties of Mo_5Si_3

Room temperature Vickers indentation tests were performed on the (100) and (001) planes of Mo_5Si_3 single crystals with different orientations of the indenter diagonal using a Micromet 4 microhardness tester. The applied load was 1000 g for 10 s. For each orientation of the indenter diagonal on each plane, five indents were made and the average values of the indentation impression and crack length measurements were obtained from the five indents. Using these averaged values, the Vickers hardness of Mo_5Si_3 single crystals along an orientation on a specific plane was calculated using: [11]

$$H = 1.8544\frac{P}{d^2} \tag{3}$$

where P is the load along the orientation on the plane and d is the impression diagonal average. The corresponding indentation fracture toughness of Mo_5Si_3 was roughly estimated from: [11]

$$K = 0.016\left(\frac{E}{H}\right)^{1/2}\frac{P}{c^{3/2}} \tag{4}$$

where c is the radial crack length average. E and H are the Young's modulus and hardness for the corresponding orientation. The impressions and cracks of the indents were further characterized using a JEOL 6300 scanning electron microscope with a field emission gun.

3. Results and discussion

The Laue back X-ray reflection patterns of the as-grown Mo_5Si_3 single crystals along the [100] and [001] axes are shown in Fig. 1. The patterns clearly indicate the 2-fold symmetry along the [100] axis and the 4-fold symmetry along the [001] axis. Chemical analysis results for Mo, Si, O, and N are tabulated in Table 1. It can be seen from Table 1 that the polycrystalline Mo_5Si_3 experienced some silicon loss during arc-melting, and single crystal Mo_5Si_3 had further silicon loss during crystal growth because of the silicon evaporation in these processes. However, these losses are minimal, being less than 0.5 at.%, so that the compositions of the alloys are still in the single phase region according to the Mo–Si phase diagram. [8] Using the data shown in Table 1, excess silicon can be added prior to the alloying process in order to precisely control the stoichiometry of Mo_5Si_3. It can also be found from Table 1 that the O and N impurities are very low in both polycrystalline and single crystal Mo_5Si_3 alloys, indicating that the techniques can be successfully employed to synthesize high purity Mo_5Si_3 single crystals. Using these crystals, the following properties of Mo_5Si_3 have been investigated.

3.1. Structural properties

Fig. 2 is the room temperature XRD pattern of $Mo_{62.75}Si_{37.25}$ ($\sim Mo_5Si_3$) powders, showing a D_{8m}-structured phase. A detailed examination of this XRD pattern indicated that there is virtually no peaks from second phases, indicating that it is indeed a single phase of Mo_5Si_3. Furthermore, this XRD pattern is compared with a previously published one, as shown in Fig. 3. [12] It can be seen from Fig. 3 that the Mo_5Si_3 XRD peaks from our study are systematically shifted to higher Bragg angles compared to the peaks from the previously published work, indicating that the lattice parameters of the $Mo_{62.75}Si_{37.25}$ ($\sim Mo_5Si_3$) alloy are smaller than the previously published results ($a = 0.96483$ nm and $c = 0.49135$ nm). Indeed, a further detailed least-square fitting to the XRD pattern shown in Fig. 2 yields lattice parameters of $a = 0.959$ nm and $c = 0.487$ nm for $Mo_{62.75}Si_{37.25}$ ($\sim Mo_5Si_3$).

3.2. Thermal properties

Thermal expansions as a function of temperature along the $\mathbf{a} = [100]$ and $\mathbf{c} = [001]$ axes for Mo_5Si_3 single crystals are shown in Fig. 4. The thermal expansion coefficients are essentially temperature independent over the measured temperature range. Linear curve fits of Fig. 4 yield the CTEs of $\alpha_a = 5.2\times10^{-6}/°C$ and $\alpha_c = 11.5\times10^{-6}/°C$ for Mo_5Si_3 single crystals. The coefficient of volume (bulk) expansion is $\beta = 2\alpha_a + \alpha_c = 21.9\times10^{-6}/°C$. The most striking feature of the CTEs of Mo_5Si_3 single crystals is their strong thermal expansion anisotropy, i.e. $\alpha_c/\alpha_a = 2.2$, which is substantially different from those of typical tetragonal high temperature structural intermetallics. The data in Table 2 list the thermal expansion values for typical tetragonal high temperature structural intermetallics, e.g. Mo_5Si_3, $MoSi_2$, and TiAl. It is found from Table 2 that $MoSi_2$ and TiAl are almost thermally isotropic, because their values of α_c/α_a are close to 1. A tentative explanation was suggested by Fu *et al.* [13] for the strong thermal expansion anisotropy of Mo_5Si_3, which might be due to the difference in interatomic bonding along the different crystallographic axes. As stated previously, the relatively strong bonded –Si–Mo–Si– chains in Mo_5Si_3 are along the [100] and [010] directions, inducing strong bonding among the atoms on the (001)

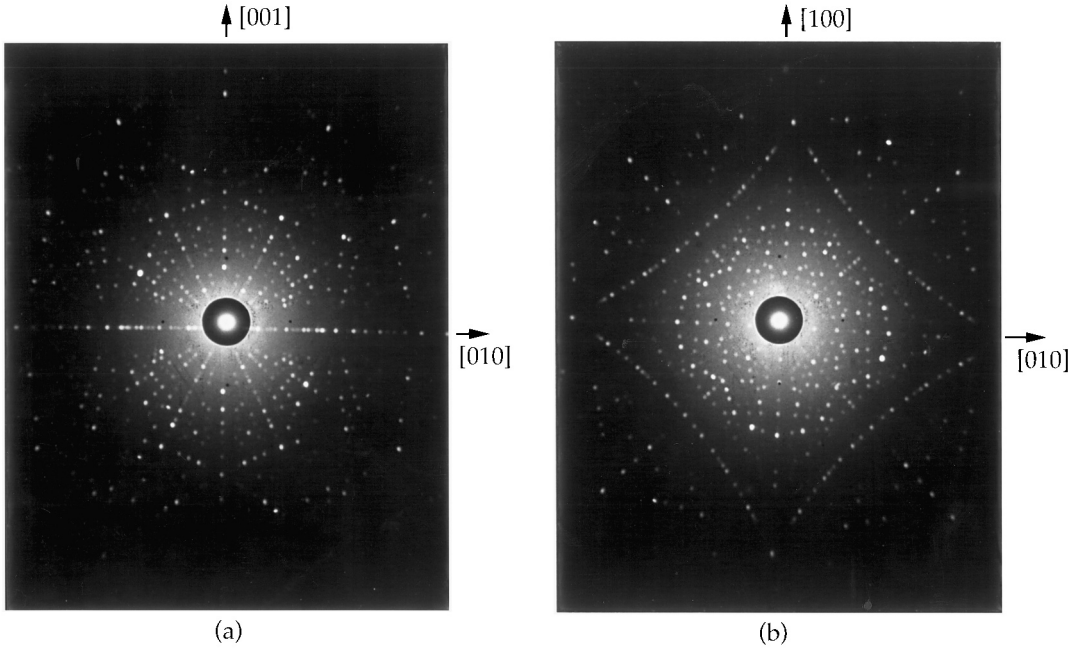

Fig. 1. Laue back X-ray reflection patterns of Mo_5Si_3 single crystals: (a) along [100] and (b) along [001].

Table 1
Chemical analysis results of the Mo_5Si_3 alloys

	Mo (at.%)	Si (at.%)	O (wppm)	N (wppm)
Starting elementals	62.50	37.50	—	—
Polycrystalline Mo_5Si_3	62.75	37.25	20	10
Single crystal Mo_5Si_3	62.92	37.08	10	10

plane, which make the thermal expansion/contraction along the [100] and [010] directions difficult to occur. Quantitative interatomic bonding results of Mo_5Si_3 obtained from a first-principles total energy and electronic structure calculation support these arguments [13]. Furthermore, thermal expansion of a solid is caused by the anharmonic effect of lattice vibration. Therefore, the strong anisotropy of thermal expansion of Mo_5Si_3 indicates that the anharmonicity is higher along the [001] direction than the [100] or [010] direction. This is consistent with the calculated results of Fu *et al.* [13] The strong thermal expansion anisotropy has a negative impact on alloy processing of Mo_5Si_3, e.g. casting and arc-melting, since the large stress at grain boundaries induced by the anisotropic thermal contraction during cooling process can induce grain boundary fracture. Indeed, significant grain boundary cracking was observed in the arc-melted buttons used in this study. Therefore, the Mo_5Si_3-based materials can only be properly studied and/or applied using: (a) single crystals, (b) polycrystals with very smaller grain sizes, or (c) Mo_5Si_3 properly alloyed by some elements, e.g. boron, to avoid the grain boundary cracking problem. [14].

3.3. Elastic properties

Fig. 5 shows a portion of the room temperature RUS spectrum of Mo_5Si_3 single crystals. A high signal-to-noise ratio and high-Q resonant peaks shown in Fig. 5 demonstrate the high quality of the specimen and the RUS measurement. Table 3 tabulates the data fitting for the RUS peaks shown in Fig. 5. A total of 70 RUS peaks in the regime 0.45–1.82 MHz were fitted and a r.m.s. error of 0.33% was obtained, indicating an excellent agreement between the experimentally measured and calculated RUS peaks. Therefore, the room temperature elastic parameters obtained from this study should be reliable.

3.3.1. Single crystal elastic parameters

Table 4 lists the single crystal elastic stiffness and compliance constants obtained from this study. Using these single crystal elastic parameters and formalism developed elsewhere, [15,16], the orientation dependence of the Young's modulus of Mo_5Si_3 is plotted in Fig. 6. It was also found using these single crystal elastic parameters [17,18] that: (a) the maximum Young's modulus of Mo_5Si_3 is along the [110] direction, $E_{max} = E_{[110]} = 364$ GPa, (b) the minimum Young's modulus of Mo_5Si_3 is along the [409] direction, $E_{min} = E_{[409]} = 294$ GPa, and (c) $E_{max}/E_{min} = 1.24$. Therefore, Mo_5Si_3 should be the stiffest along [110] and the most compliant along [409] in response to tension or compression loading within the elastic regime.

Similarly, the orientation dependence of the shear modulus of Mo_5Si_3 is obtained and shown in Fig. 7. It can be seen from Fig. 7 that the lowest shear modulus is

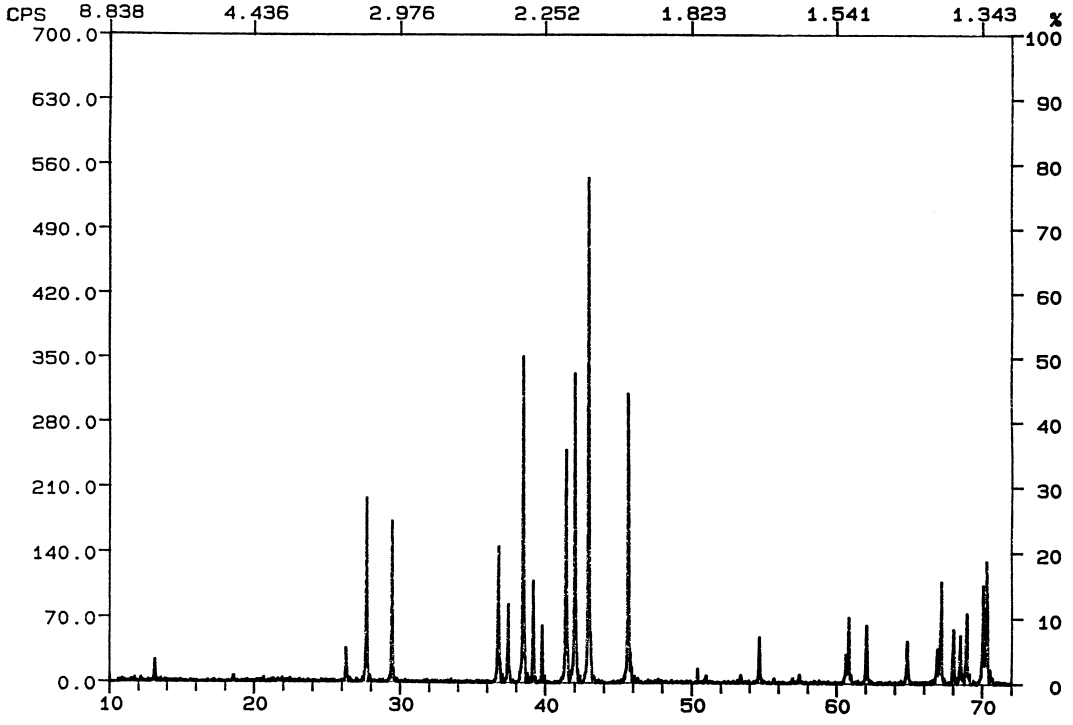

Fig. 2. The room temperature XRD pattern of $Mo_{62.75}Si_{37.25}$ ($\sim Mo_5Si_3$) powders, showing a D_{8m}-structured phase.

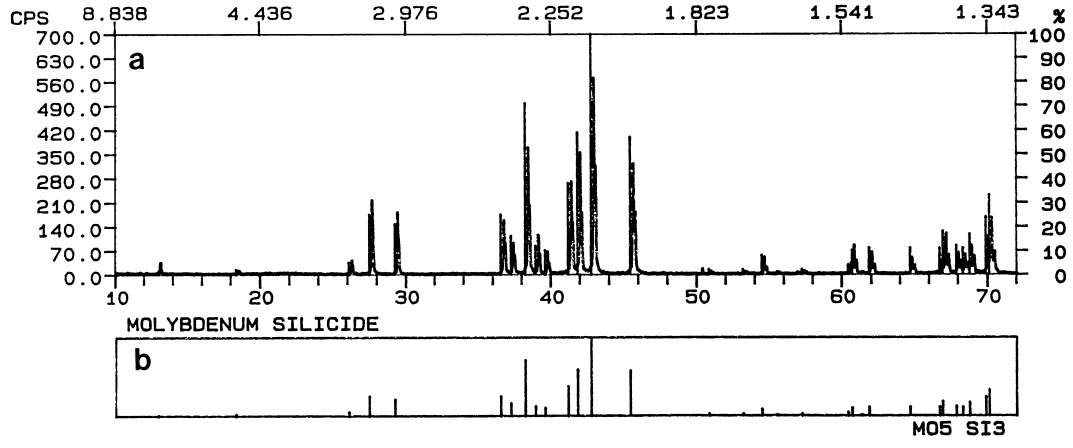

Fig. 3. A comparison between the XRD patterns of Mo_5Si_3: (a) the XRD pattern from this study and (b) the XRD pattern from a previously published study.

110 GPa on the (001) plane along any direction, on the (100) plane along [001], and on the (110) plane along [001]. On the other hand, the shortest Burgers vector exists on the (100) plane along [001] and on the (110) plane along [001] in Mo_5Si_3, i.e. $\mathbf{b}=[001]$. Therefore, it is reasonable to predict that the possible dislocation slip systems in Mo_5Si_3 are (100)/[001] and/or (110)/[001]. Furthermore, a comprehensive theoretical prediction of the deformation modes should be performed using the lattice and crystallographic data and the single crystal elastic parameters. [19]. Of course, all of these postulates need to be verified by experimental observations. This work is currently underway.

Single crystal elastic parameters can also provide valuable insight into the characteristics of interatomic bonding through certain criteria, e.g. Cauchy's relationships, elastic isotropic factors, Poisson's ratios, and c_{33}/c_{11} ratio. The Cauchy's relationships between the elastic stiffness constants for tetragonal crystals with central forces are [20]

$$c_{13} = c_{14} \quad \text{and} \quad c_{12} = c_{66}$$

The data in Table 4 indicate that the Cauchy's relationships do not hold true for Mo_5Si_3 and this fact implies

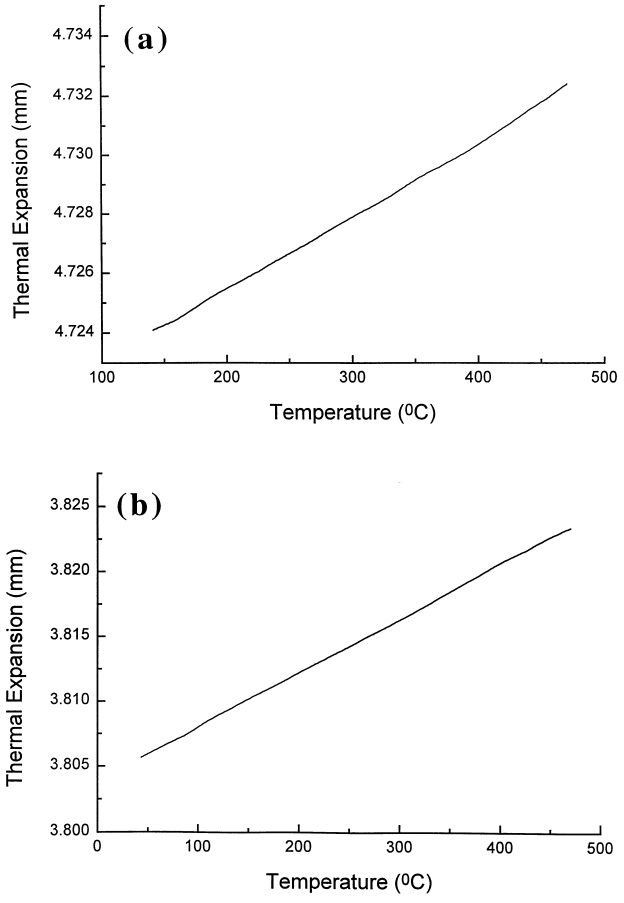

Fig. 4. The thermal expansion as a function of temperature for Mo_5Si_3 single crystals: (a) along the [100] axis and (b) along the [001] axis.

Table 2
The thermal expansion data of typical tetragonal high temperature structural intermetallics

Materials	α_a (10^{-6}/°C)	α_c (10^{-6}/°C)	β (10^{-6}/°C)	α_c/α_a
Mo_5Si_3	5.2	11.5	21.9	2.21
$MoSi_2$[a]	8.2	9.4	25.8	1.15
TiAl[b]	9.7	9.3	32.6	0.96

[a] Refs. [24,17].
[b] Ref. [18].

that the interatomic forces in Mo_5Si_3 are non-central. However, there are relatively less difference between c_{13} and c_{44} and between c_{12} and c_{66} for Mo_5Si_3 comparing with those of $C11_b$ and C40 transition metal disilicides, [16] where the Cauchy's relationships do not hold true by more than a factor of 3 in some cases.

The elastic anisotropy factors of Mo_5Si_3 are tabulated in Table 5, along with those of typical tetragonal high temperature structural intermetallics, e.g. $MoSi_2$ and TiAl. Table 5 suggests that the elastic anisotropy factors of Mo_5Si_3 are closer to unity than those of $MoSi_2$ and TiAl, although these factors still indicate that Mo_5Si_3 is anisotropic in elasticity.

The Poisson's ratios of Mo_5Si_3 are tabulated in Table 6, along with those of the typical tetragonal high temperature structural intermetallics, e.g. $MoSi_2$ and TiAl. The data in Table 6 clearly demonstrate that the Poisson's ratios of Mo_5Si_3 single crystals are substantially larger than those of $MoSi_2$.

The c_{33} and c_{11} relationship of Mo_5Si_3 is different from that of $C11_b$ transition metal disilicides, e.g. $MoSi_2$ and WSi_2. For Mo_5Si_3, $c_{33} < c_{11}$ with $c_{33}/c_{11} = 0.87$. However, for $MoSi_2$ and WSi_2, $c_{33} > c_{11}$ with $c_{33}/c_{11} = 1.26$. [16]. This is related to the bonding strength along the [100] and [001] axes in the two intermetallic phases. As described above, the strongly bonded –Si–Mo–Si– chains are along [100] and [010] directions and the weakly bonded –Mo–Mo– and –Si–Si– chains are along [001] in Mo_5Si_3, therefore, c_{11} should be larger than c_{33} in this compound. On the other hand, the strongly bonded –Si–Mo–Si– chains are along [001] and the weakly bonded –Mo–Mo– and –Si–Si– chains are along [100] and [010] directions in $MoSi_2$ and WSi_2, therefore, c_{33} should be larger than c_{11} in these phases. It is generally true for tetragonal systems that a quantitative comparison between c_{11} and c_{33} may provide a qualitative comparison between the bonding strength along the [100] and [001] axes.

Finally, the single crystal elastic constants of Mo_5Si_3 can be used to determine its mean sound velocity and elastic Debye temperature (Θ_D) using Eq. (1) and Eq. (2). These values are listed in Table 7 and compared with those of $C11_b$ and C40 transition metal disilicides. Table 7 indicates that Mo_5Si_3 has a lower Debye temperature although it has a higher melting point among the three silicides. Therefore, Mo_5Si_3 has a Θ_D/T_m ratio of 0.23, which is significantly lower than those of $C11_b$ and C40 transition metal disilicides. This fact may imply two points for the thermal atomic vibrations in Mo_5Si_3: (a) the atomic vibrations have lower frequencies and (b) the atomic vibrations reach a large amplitude at a lower temperature. The impacts of these characteristics on the mechanical behavior of Mo_5Si_3, e.g. brittle-to-ductile transition temperature (BDTT), need to be investigated through mechanical testing.

3.3.2. *Polycrystalline isotropic elastic moduli*

The isotropic elastic moduli of Mo_5Si_3 can be derived by the Voigt, Reuss, or Hill approximation and compared with those of the constituent elements and the average values derived from the rule of mixtures. These values are given in Table 8. It can be seen that the isotropic elastic moduli and the Poisson's ratio of polycrystalline Mo_5Si_3 are close to those of Mo, especially the shear and Young's moduli. The Poisson's ratio of polycrystalline Mo_5Si_3 is 0.278 as shown in Table 8, which is substantially larger than $\nu \sim 0.15$ of the $C11_b$ transition metal disilicides and $\nu \sim 0.19$ of the C40 transition metal disilicides. [16]

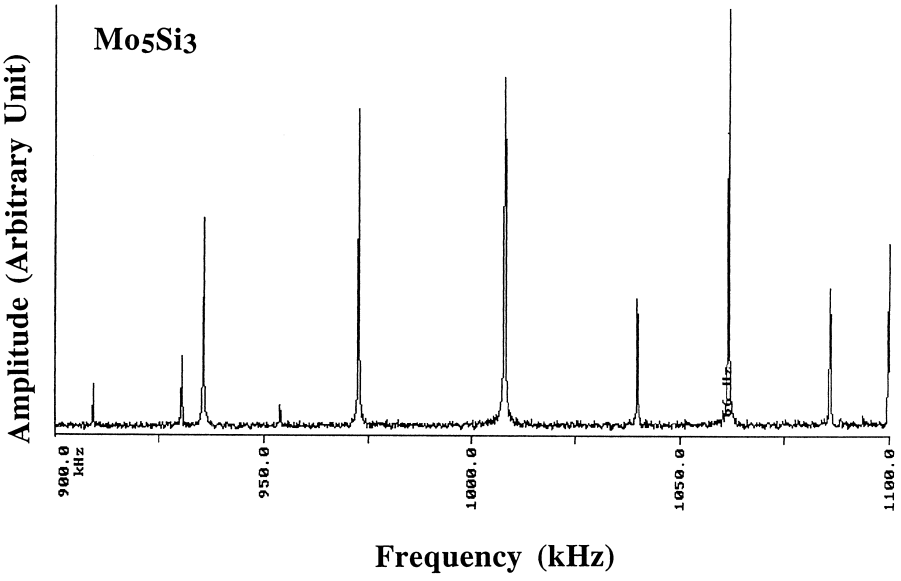

Fig. 5. A portion of the room temperature RUS spectrum of Mo_5Si_3 single crystals.

Table 3
Mo_5Si_3 RUS data fitting to the RUS peaks shown in Fig. 5. $f_{exp.}$ and $f_{cal.}$ are the experimentally measured and calculated frequencies, respectively

Number	$f_{exp.}$ (MHz)	$f_{cal.}$ (MHz)	Error (%)
1	0.909070	0.912977	0.43
2	0.930420	0.928968	−0.16
3	0.935620	0.938628	0.32
4	0.953760	0.954692	0.10
5	0.972710	0.971660	−0.11
6	1.007800	1.007425	−0.04
7	1.039800	1.042994	0.31
8	1.061800	1.059444	−0.22
9	1.085900	1.079995	−0.54
10	1.099800	1.094000	−0.53

Table 4
Room temperature elastic stiffness and compliance constants of Mo_5Si_3 single crystals

(i,j)	11	33	13	12	44	66
c_{ij} (GPa)	446	390	140	174	110	140
s_{ij} (10^{-3} GPa^{-1})	2.80	3.06	−0.69	−0.87	9.09	7.14

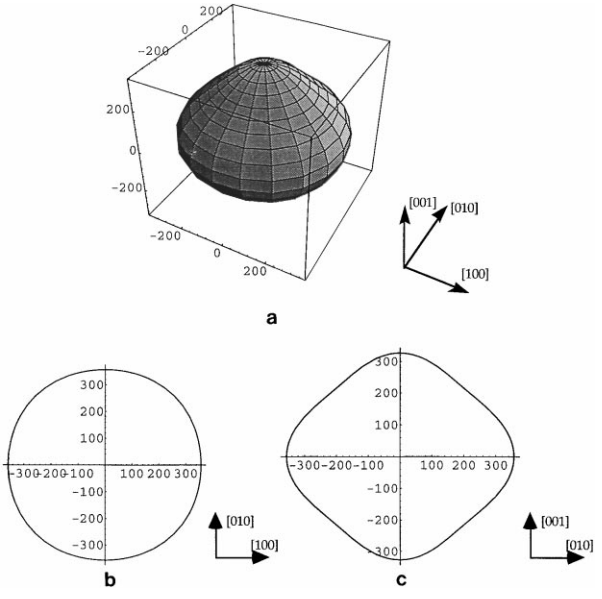

Fig. 6. The orientation dependence of the Young's modulus of Mo_5Si_3 single crystals: (a) the 3-dimensional plot, (b) the Young's moduli along the directions perpendicular to [001], and (c) the Young's moduli along the directions perpendicular [100].

The isotropic elastic moduli of Mo_5Si_3 can be used to qualitatively examine its mechanical behavior, for example, using the Pugh criterion. [21] Based on the Pugh criterion, an alloy should be relatively ductile if it has a large K/G ratio. From Table 8, Mo_5Si_3 has a K/G value of 1.92, which is larger than that of Si (1.42) and slightly lower than that of Mo (2.08). On the other hand, $C11_b$ $MoSi_2$ has a K/G value of 1.09 and C40 $NbSi_2$ has a K/G value of 1.25. Although the Pugh criterion should be applied to the alloys with the same crystal structure, the comparison of these ratios may still indicate that Mo_5Si_3 has a promising mechanical behavior. Of course, the true mechanical properties of Mo_5Si_3 are determined by its deformation modes/mechanisms. Further mechanical testing is needed to investigate the deformation mechanisms and mechanical properties of Mo_5Si_3.

The specific Young's modulus (the ratio of the Young's modulus to the density of a material) is an important engineering design parameter for materials in

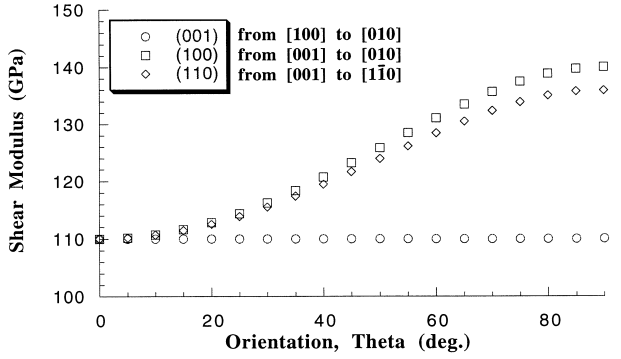

Fig. 7. The orientation dependence of the shear moduli of Mo_5Si_3 single crystals on the (001) plane from [110] to [010], the (100) plane from [001] to [010], and the (110) plane from [001] to [1$\bar{1}$0].

Table 5
Elastic anisotropy factors of Mo_5Si_3, $MoSi_2$ and TiAl

Anisotropy Factors	Mo_5Si_3	$MoSi_2$	TiAl
c_{33}/c_{11}	0.874	1.255	0.946
c_{13}/c_{12}	0.804	0.796	0.857
$2c_{44}/(c_{11}-c_{12})$	0.809	1.401	2.963
$2c_{66}/(c_{11}-c_{12})$	1.029	1.345	1.235

Table 6
The Poisson's ratios of Mo_5Si_3, $MoSi_2$ and TiAl

Poisson's Ratios	Mo_5Si_3	$MoSi_2$	TiAl
$\nu_{31}=-s_{13}/s_{33}$	0.2255	0.1780	0.2900
$\nu_{12}=-s_{12}/s_{11}$	0.3107	0.2570	0.2609
$\nu_{13}=-s_{13}/s_{11}$	0.2464	0.1360	0.3188

Table 7
The mean sound velocities and the Debye temperatures of Mo_5Si_3, $MoSi_2$ and $NbSi_2$

Materials	Density ($g\,cm^{-3}$)	v_m ($m\,s^{-1}$)	Θ_D (K)	Θ_D/T_m
Mo_5Si_3	8.19	4317	566	0.2307
$MoSi_2$[a]	6.30	6097	760	0.3314
$NbSi_2$[a]	5.70	5727	688	0.3137

[a] Ref. [16].

Table 8
The isotropic elastic moduli and Poisson's ratio of Mo_5Si_3. K is the bulk modulus, G the shear modulus, E the Young's modulus, and ν the Poisson's ratio

Materials	K (GPa)	G (GPa)	E (GPa)	ν
Mo[a]	259.7	125.0	323.2	0.293
Si[a]	97.9	68.1	162.9	0.225
Mo_5Si_3: averaged values	199	104	263	0.268
Mo_5Si_3: Hill approximation	242	126	323	0.278

[a] Compiled from the data in Refs. [24,25].

aerospace applications. Mo_5Si_3 has a specific Young's modulus of about 40 GPa/($g\,cm^{-3}$), which is higher than those of nickel aluminides (25–32 GPa/($g\,cm^{-3}$)), comparable with titanium aluminides (30–50 GPa/($g\,cm^{-3}$)), and lower than those of $MoSi_2$ and $NbSi_2$ (65–70 GPa/($g\,cm^{-3}$)).

3.4. Mechanical properties

Fig. 8(a) shows the orientation dependence of the room temperature Vickers hardness, calculated from Eq. (3), on the (100) and (001) planes of Mo_5Si_3 single crystals. The hardness on these planes of Mo_5Si_3 is not

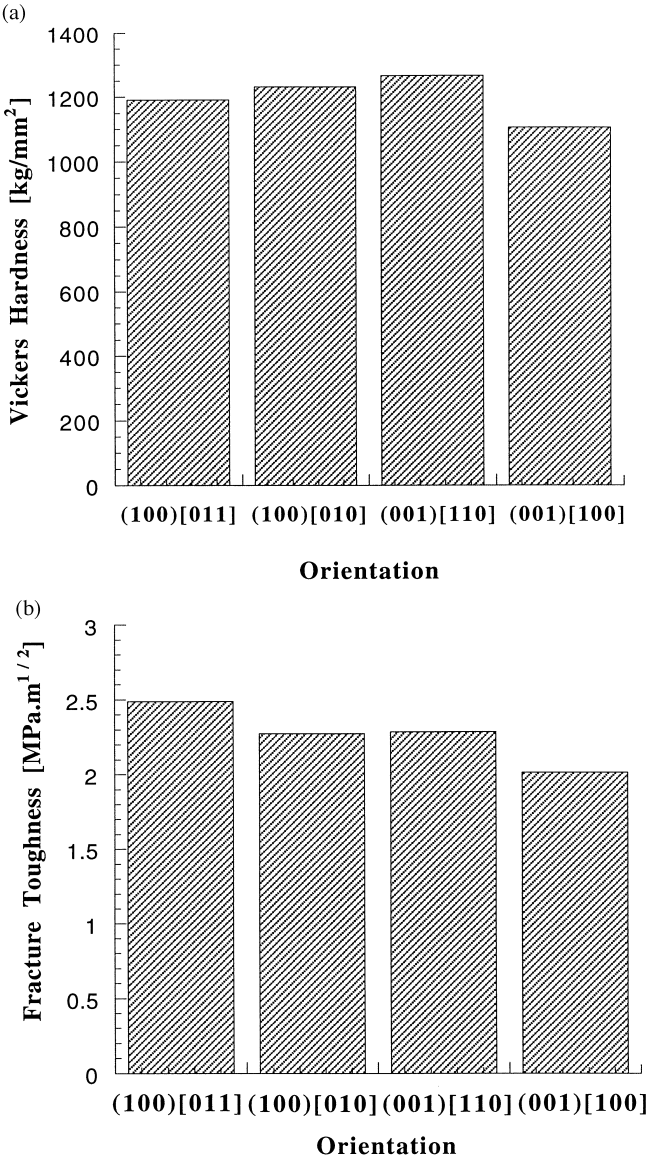

Fig. 8. The orientation dependence of (a) the room temperature Vicker's hardness and (b) the indentation fracture toughness on the (100) and (001) planes of Mo_5Si_3 single crystals. (100)[011] means the indentation is on the (100) plane and one indenter edge is parallel to [011].

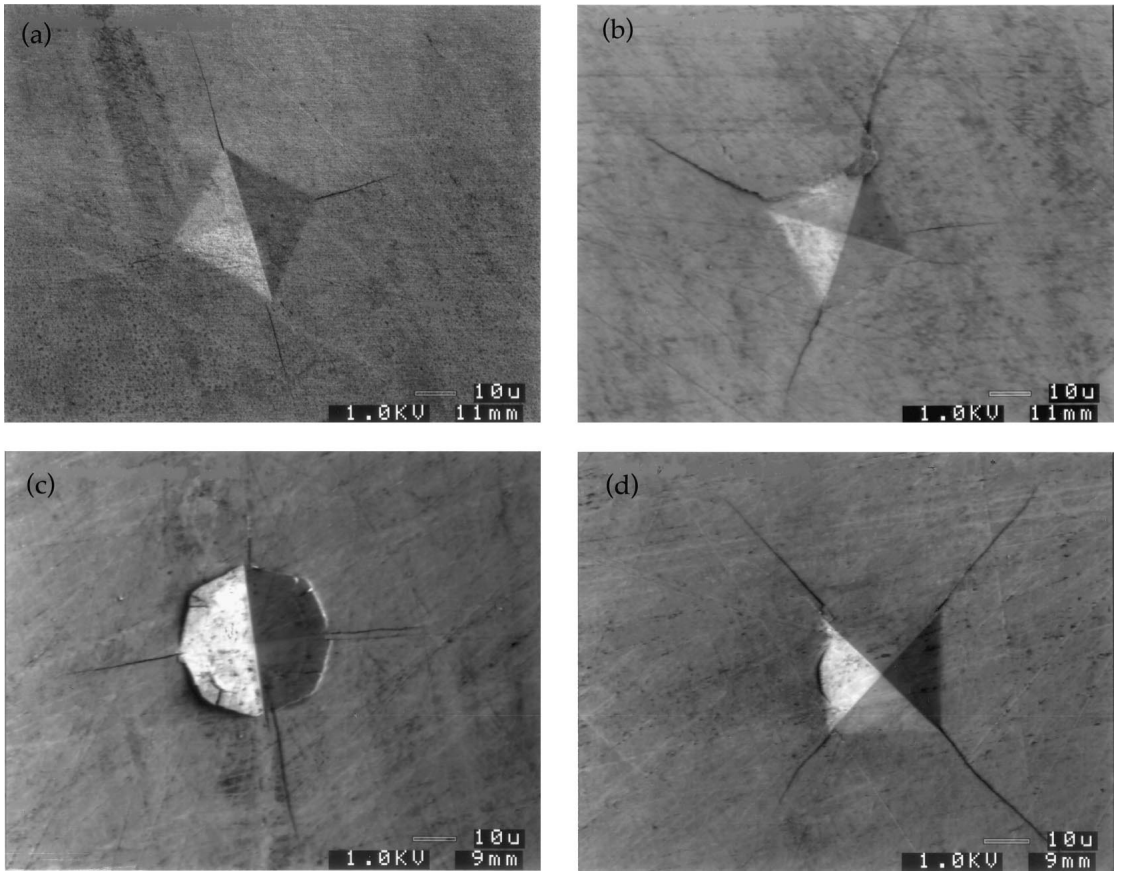

Fig. 9. SEM micrographs of the indentation impressions and the associated cracks on Mo_5Si_3 single crystals: (a) on the (100) plane and one indenter edge is parallel to [011], (b) on the (100) plane and one indenter edge is parallel to [010], (c) on the (001) plane and one indenter edge is parallel to [110], and (d) on the (001) plane and one indenter edge is parallel to [100].

significantly orientation dependent and the hardness has large values around 1200 $kg\,mm^{-2}$, which are substantially higher than those of $MoSi_2$ single crystals (600–900 $kg\,mm^{-2}$, depending on the testing orientations) [22] and those of $NbSi_2$ single crystals (~700 $kg\,mm^{-2}$, depending on the testing orientations). [23] It is interesting to note that there is a noticeable difference (~10%) between the hardness on the same (001) plane but with different indenter diagonal orientations.

Fig. 8(b) demonstrates the orientation dependence of the indentation fracture toughness, roughly estimated from Eq. (4), on the (100) and (001) planes of Mo_5Si_3 single crystals. It can be seen from Fig. 8(b) that the room temperature indentation fracture toughness on these planes of Mo_5Si_3 is within 2–2.5 $MPa\sqrt{m}$, showing a minor orientation dependence. These values are comparable with those of $MoSi_2$ single crystals on some orientations. [22] It is also interesting to note that there is a noticeable difference (~10%) between the fracture toughness on the same (001) plane but with different indenter diagonal orientations.

SEM micrographs of the indentation impressions and the associated cracks on the (100) and (001) planes with two indenter diagonal orientations are shown in Fig. 9. Dislocation slip traces are not observed near the indent impressions, suggesting that dislocation slip may not be operative for these mechanical loading at ambient temperature in Mo_5Si_3. It can be seen from Fig. 9 that the cracks are generated at the four corners of the indent impression and no secondary cracks are observed for Mo_5Si_3. On the other hand, cracks may be generated at only two corners of some indent impressions and substantial secondary cracks are observed for $MoSi_2$. [22] Therefore, the fracture behavior of Mo_5Si_3 may be less anisotropic than that of $MoSi_2$. The most striking feature is that the indentation shapes on the (001) plane are completely different, as shown in Fig. 9(c) and (d), for the two different indenter diagonal orientations. This may be responsible for the noticeable differences (~10%) in the hardness and fracture toughness for these indentations as mentioned above. It is important to understand the reason(s) why such a significant difference exists in the plastic response to the same loading by considering the elastic properties and examining the plastic deformation mechanisms in Mo_5Si_3. This work is currently under way.

4. Conclusions

Ultra-high temperature intermetallic, Mo_5Si_3, has been studied by single crystal growth, physical property measurement and mechanical testing. Three primary conclusions have been reached:

1. High purity Mo_5Si_3 single crystals have been synthesized by both the optical floating zone and the Czochralski methods. Alloy processing and single crystal growth result in a minimal silicon loss of less than 0.5 at.%. The oxygen and nitrogen impurities are minimal (~10 wppm) in the single crystals.
2. Physical properties of Mo_5Si_3 have been experimentally measured, including:
   (a) Mo_5Si_3 has a D_{8m} structure with lattice parameters of $a = 0.959$ nm and $c = 0.487$ nm, which are slightly smaller than the previously published results.
   (b) Mo_5Si_3 has the CTEs of $\alpha_a = 5.2\times10^{-6}/°C$ and $\alpha_c = 11.5\times10^{-6}/°C$, showing a strong thermal expansion anisotropy ($\alpha_c/\alpha_a = 2.2$). The strong thermal expansion anisotropy is related to the difference in bonding along the [100] and [001] directions. The thermal expansion anisotropy results in grain boundary cracking in the alloy processing of Mo_5Si_3.
   (c) Mo_5Si_3 has room temperature single crystal elastic constants of $c_{11} = 446$, $c_{33} = 390$, $c_{13} = 140$, $c_{12} = 174$, $c_{44} = 110$, and $c_{66} = 140$ GPa, respectively. Analysis of the Cauchy's relationships, Poisson's ratios, and elastic anisotropic factors indicate that Mo_5Si_3 is less anisotropic in elasticity than typical tetragonal intermetallics, e.g. $MoSi_2$ and TiAl. The orientation dependence of the Young's modulus reveals that the Mo_5Si_3 is the stiffest along [110] and the most compliant along [409] under tension/compression loading within elastic regime. The orientation dependence of the shear modulus suggests that the (100)/[001] and/or (110)/[001] are favorable dislocation slip systems in Mo_5Si_3.
3. Results of the room temperature Vickers indentation tests on the (100) and (001) planes reveal that Mo_5Si_3 single crystals have a hardness of around 1200 $kg\,mm^{-2}$, which is larger than that of $MoSi_2$, and a fracture toughness above 2 $MPa\sqrt{m}$, which is comparable to that of $MoSi_2$. Plastic responses (the shape of indent impression) to the (001) indentations with two different indenter diagonal orientations are significantly different, resulting in a noticeable difference in the corresponding hardness and fracture toughness.

Acknowledgements

This work has been supported by the US Department of Energy, Basic Energy Sciences (Division Of Materials Science).

References

[1] Liu CT. In: Darolia R, Lewandowski JJ, Liu CT, Martin PL, Miracle DB, Nathal MV, editors. Structural intermetallics. Warrendale, PA: TMS, 1993:365.
[2] Darolia R. In: Darolia R, Lewandowski JJ, Liu CT, Martin PL, Miracle DB, Nathal MV, editors. Structural intermetallics. Warrendale, PA: TMS, 1993:495.
[3] Gibala R, Chang H, Czarnik C, Edwards K, Misra A. In: Darolia R, Lewandowski JJ, Liu CT, Martin PL, Miracle DB, Nathal MV, editors. Structural intermetallics. Warrendale, PA: TMS, 1993:561.
[4] Yamaguchi M, Inui H. In: Darolia R, Lewandowski JJ, Liu CT, Martin PL, Miracle DB, Nathal MV, editors. Structural intermetallics. Warrendale, PA: TMS, 1993:127.
[5] Petrovic JJ. MRS Bulletin 1993;XVIII:35.
[6] Maloy SA, Mitchell TE, Hauer AH. Acta Metall Mater 1995;43:657.
[7] Pope DP, Chu F. In: Darolia R, Lewandowski JJ, Liu CT, Martin PL, Miracle DB, Nathal MV, editors. Structural intermetallics. Warrendale, PA: TMS, 1993:637.
[8] Massalski TB, editor. Binary alloy phase diagram. Pittsburgh: ASM, 1986:2666.
[9] Migliori A, Sarrao JL, Visscher WM, Bell TM, Lei Ming, Fisk Z, Leisure RG. Physica 1993;B183:1.
[10] Blackman M. In: Handbuch der physik, vol. 7. Flugge S, editor. Berlin: Springer, 1955:325.
[11] Anstis GR, Chantyikul P, Lawn BR, Marshall DB. J Am Ceram Soc 1981;64:533.
[12] JCPDS-ICDD, No. 34-371, 1993.
[13] Fu CL, et al. Intermetallics, submitted.
[14] Liu CT, Schneible J, Yoo MH. Private communications.
[15] He Y, Schwarz RB, Migliori A, Whang SH. J Mater Res 1995;10:1187.
[16] Chu F, Lei M, Maloy SA, Petrovic JJ, Mitchell TE. Acta Mater 1996;44:3035.
[17] Thomas O, Senateur JP, Madar R, Laborde O, Rosencher E. Solid State Commun 1985;55:629.
[18] He Y, Schwarz RB, Darling T, Hundley M, Whang SH, Wang ZM. Mater Sci Eng A, in press.
[19] Yoo MH. Phil Mag 1993;A68:1295.
[20] Nye JF. Physical properties of crystals. London: Oxford University Press, 1979.
[21] Pugh SF. Phil Mag 1954;54:823.
[22] Peralta P, Maloy SA, Chu F, Petrovic JJ, Mitchell TE. Scripta Mater 1997;37:1599.
[23] Maloy SA, Chu F, Petrovic JJ, Mitchell TE. In: Soboyejo WO, Fraser HL, Srivatsan TS, editors. Deformation and fracture of ordered intermetallic materials III. Warrendale, PA: TMS, 1996.
[24] Simmons G, Wang H. Single crystal elastic constants and calculated aggregate properties: a handbook. Cambridge, MA: MIT Press, 1971.
[25] Hirth JP, Loathe J. Theory of dislocations. New York: John Wiley, 1982.